ELSEVIER

Contents lists available at ScienceDirect

Materials Today Energy

journal homepage: www.journals.elsevier.com/materials-today-energy/



Sulfur confined MXene hosts enabling the use of carbonate-based electrolytes in alkali metal (Li/Na/K)-sulfur batteries



Rahul Pai ^a, Varun Natu ^b, Maxim Sokol ^c, Michael Carey ^b, Thomas Greszler ^d, Michel W. Barsoum ^{b, **}, Vibha Kalra ^{a, *}

- ^a Department of Chemical and Biological Engineering, Drexel University, 3141 Chestnut Street, Philadelphia, PA 19104, USA
- ^b Department of Material Science Engineering, Drexel University, 3141 Chestnut Street, Philadelphia, PA 19104, USA
- ^c Department of Material Science and Engineering, Tel Aviv University, Ramat Aviv 6997801, Tel Aviv, Israel

ARTICLE INFO

Article history: Received 9 September 2021 Received in revised form 23 March 2022 Accepted 24 March 2022 Available online 5 May 2022

Keywords: Energy 2D Intercalation Chalcogen Carbides

ABSTRACT

Room-temperature alkali metal—sulfur batteries are promising alternatives to lithium-ion batteries because of their high capacity and low inherent cost. Herein, we report MXene (Ti_3C_2Tx) as a host to confine sulfur (S_8) , enabling the use of commercialization-friendly carbonate electrolyte in metal—sulfur batteries. The multilayer MXene structure provides tunable spacing for S_8 confinement, and its unique interlayer spacing prevents adverse polysulfide-carbonate reactions.

© 2022 Elsevier Ltd. All rights reserved.

1. Introduction

From the great contributions by Goodenough et al. to its practical use in commercial electric vehicles, Li-ion batteries have come a long way with substantial developments in the past three decades [1,2]. The Li-ion chemistry has now reached its theoretical limit, and new battery breakthroughs are necessary for the broad deployment of electric vehicles. Sulfur (S)-based batteries are considered to be some of the most promising "beyond Li-ion" battery systems [3] because elemental S can exhibit a fivefold higher theoretical capacity than state-of-the-art Li-ion cathodes and is abundant in nature, inexpensive, and environmentally harmless [4]. The consistent developments have led to the maturation of this system, which now offers the capability to supersede the intrinsic limits of Li-ion technology along with cost reductions as well as environmental benignity. However, the practicality of S-batteries is hindered by several challenges. The key issues

E-mail addresses: barsoumw@drexel.edu (M.W. Barsoum), vk99@drexel.edu (V. Kalra).

investigated in the literature in this past decade are the insulating nature of S; the inevitable S volume change during cycling [5–7]; and the dissolution of intermediate reaction products, polysulfides, causing the notorious shuttling effect and rapid capacity fade during cycling [8–10].

So far, polysulfide shuttling has received the most attention, and a majority of studies in metal-S batteries in the past decade have focused on the development of strategies to mitigate this effect, which is an inherent phenomenon observed in ether-based electrolytes [11]. A much less discussed but debilitating drawback for the commercial viability of Li-S batteries is the use of the ether electrolyte itself. Ether-based solvents are highly volatile and have low flash points posing a significant risk of operating such batteries beyond room temperatures [12]. In addition, lithium nitrate (LiNO₃), an important additive in ether electrolyte to stabilize Li metal surface, causes degassing above 40°C, and therefore, it does not pass test 2 of UN38.3 Transport of Dangerous Goods Certification, further hindering their practicality due to safety and transport concerns [13]. Carbonate-based electrolytes, used in traditional Liion batteries, have various advantages over their ether-based counterparts. The three decades of research on the former have shown that they have low melting points, lower costs, and higher

^d Space and Defense Division, Saft America, Cockeysville, MD, USA

^{*} Corresponding author.

^{**} Corresponding author.

oxidation potentials [14]. However, the S-cathode is not compatible with the conventional carbonate electrolytes because during discharge, the polysulfide anions react with the carbonate solvent irreversibly because of a strong nucleophilic reaction [15]. To avoid the latter recent studies suggest that microporous carbon as a host can effectively suppress the direct contact between the solvent molecule in carbonate-based electrolytes and S (or polysulfide intermediates) molecule because of pore size limitations [16—18].

MXenes are a decade-old class of two-dimensional (2D) carbides and/or nitrides discovered in 2011 by Naguib et al. [19]. These 2D materials are so-called because they are derived by selectively etching A (group 13 or 14 elements) from the parent MAX phase in aqueous acid and organic solvents [20,21]. MXenes have a general formula $M_{n+1}X_nT_z$, where M stands for an early transition metal, X stands for C, or N and T stands for chemical terminations such as -0, -0H, and -F surface groups that replace the Al atoms upon etching [20].

The Ti-based MXene, Ti₃C₂T₂, obtained by etching Ti₃AlC₂, has shown unique properties, such as high metallic conductivity (>5,000 S/cm), high active surface area, and sufficient environmental stability [22–25]. The developed MXenes can be tuned with various surface functional groups as required for its applications adding to its versatility [26–30]. In addition to its unique properties, the interlayer spacing of MXenes can be controllably tuned [22,31–33]. Physical mixing of MXene and S resulting in sandwichtype architecture has shown appealing performances in Li-S systems [34,35]. However, these systems cannot function in carbonate-based electrolytes because of undesirable reactions alludded to above. Herein, for the first time, we demonstrate the use of MXene host in carbonate electrolyte-based Li-S batteries. In addition, we also demonstrate the versatility of these developed cathodes in Na-S and K-S batteries, also using carbonate electrolyte.

Alternate metal chemistries, beyond lithium, such as Na and K, are interesting, as they exhibit similar advantages as Li-S batteries in addition to increased abundance and lower cost over Li. However, Na/K-S batteries face all the same challenges as Li-S systems such as rapid capacity fade and low electrochemical utilization. In addition, they also suffer from more sluggish redox kinetics due to the larger ionic radius of Na⁺ (0.102 nm) and K⁺ (0.138 nm) vs Li⁺ (0.076 nm), resulting in the formation of only Na₂S₂ and K₂S₃ as the final discharge product, compared with Li₂S in the Li-S system. Furthermore, the larger ionic size results in significantly higher volume expansion of 170% in Na-S, for example, vs. 80% in Li-S, further deteriorating cathode integrity [36]. Such aggravated challenges often result in lower achieved capacity and stability in reported works [5,37,38], making efficient cathode design even more critical for such batteries.

In this work, to enable the use of carbonate electrolytes in Li/Na/ K-S batteries, we have focused on the utilization of 2D MXene nanosheets as a host to confine sulfur within the interlayer spacings with the objective to trigger ion desolvation, mitigating adverse carbonate-sulfur reactions. As mentioned previously, herein, for the first time, we fabricate MXene-based sulfur cathodes that successfully operate in carbonate electrolytes in Li/Na/K systems. Moreover, this is the first-ever study that demonstrates the use of MXenes in any K-S battery system. To synthesize our cathodes, we first treated multilayered (ML) MXenes with di (hydrogenated tallow) benzyl methyl ammonium chloride (DHT) to increase the interlayer spacing to facilitate S intercalation into the MXene interlayer gaps [22]. Furthermore, they were subjected to a thermal treatment to intercalate sulfur in between the layers. The synthesized samples were characterized via scanning electron microscopy (SEM), transmission electron microscopy (TEM)/energy-filtered transmission electron microscopy mapping (EFTEM)/energydispersive X-ray spectroscopy (EDS), X-ray diffraction (XRD), X-ray photoelectron spectroscopy (XPS), and thermogravimetric analysis (TGA) to investigate the presence of S in the MXene sheets. Detailed electrochemical characterizations were conducted in three different sulfur batteries using Li, Na, and K as anodes exhibiting successful and stable redox in a carbonate electrolyte.

2. Experimental

2.1. Materials

2.1.1. Material for synthesis

Titanium carbide (TiC; 99.5%, 2 μ m), aluminum (Al; 99.5%, 325 mesh), and titanium (Ti; 99.5%, 325 mesh) and LiF (99.5%, 325 mesh) were purchased from Alfa Aesar. 12 M HCl was purchased from Fisher Scientific, and DHT (80%) was purchased from Alfa Chemistry.

2.1.2. Materials for electrochemistry

Sulfur (99.5%, sublimed, catalog number AC201250025) was purchased from Fisher Scientific. Battery-grade ethylene carbonate, diethyl carbonate, propylene carbonate, fluoro-ethylene carbonate, lithium hexafluorophosphate, sodium hexafluorophosphate, and potassium hexafluorophosphate were purchased from Sigma Aldrich.

2.2. Synthesis

2.2.1. Synthesis of MAX powder (Ti₃AlC₂)

Parent Ti_3AlC_2 powders were synthesized by mixing titanium carbide (TiC), aluminum (Al), and titanium (Ti) powders in a molar ratio of 2:1.05:1, respectively. The mixed powders were ball milled at 100 rpm for 24 h and then heated under argon (Ar) flow at 1,350°C for 2 h. It should be noted that the ball milling at slow speed was only used for homogenous mixing; no particle size reduction or reactions are occurring. The heating and cooling rates were set at 5°C/min. The resulting blocks were ground to powders using a milling bit on a drill press. The milled powders were passed through a 400-mesh (particle size <38 μ m) sieve for further experiments.

2.2.2. Synthesis of MXene $(Ti_3C_2T_z)$ and DHT treatment

First, 1 g of LiF was dissolved in 10 mL of 12 M HCl, after which 1 g of the Ti_3AlC_2 powder was slowly added to the solution. Then it was stirred for 24 h at 35°C and 300 rpm. The resulting solution was later transferred into a 50 mL centrifuge tube, and deionized (DI) water was added to completely fill the remaining volume. It was then centrifuged at 3,500 rpm/2,300 rcf for 1 min, and the resulting clear supernatant was discarded. This washing was repeated several times until the pH of the solution was \approx 7. Afterward, the sediment was divided into two equal parts. One part was dried in a vacuum at 100° C for 12 h and is labeled as normal untreated MXene (NMX). In the second part, 40 mL of a 20-mM preprepared solution of DHT in a 50:50 (v:v) of water, and ethanol was added and allowed to mix for 12 h at room temperature (RT). After mixing, all of the powders were washed with DI water three times. The resulting DHT-MXene or DMX was dried in a vacuum at 100° C for 12 h

2.2.3. Synthesis of MXene-sulfur composite

2.2.3.1. Moderate weight percentage electrodes, 50 wt %. In a typical synthesis, 0.1 g of dried DMX was mixed with 0.1 g of sulfur and ground with mortar-pestle until the mixture was uniform. Later, this solid mixture was transferred in a glass test tube and then into an argon-filled glove box, where the top was physically closed with a coin cell spacer and sealed with Teflon tape. This assembly was further loaded in a house-made reactor consisting of a 6-inch

stainless steel (SS) pipe fitting and sealed in the glove box with pipe caps and then transferred out. Furthermore, this reactor was loaded in a horizontal tube furnace at 350°C for 3 h at a rate of 2°C/min in an argon environment. The mixture after thermal treatment will henceforth be referred to as a DMX/S. Fig. 1 is a schematic of what occurs during the thermal treatment.

2.2.4. Synthesis of DMX/S composite electrode

A cathode was fabricated using a slurry method. Briefly, the slurry was prepared by mixing 80 wt% of vacuum-dried DMX/S with 10 wt% conductive carbon (Alfa Aesar, Super P) and 10 wt% battery-grade polyvinylidene fluoride (PVDF) binder (MTI corp, USA). DMX/S, conductive carbon, and PVDF were hand-ground with mortar and pestle till the composite turned uniform. Later, N-Methyl-2-pyrrolidone (TCI, USA) was slowly added until required visible consistency and uniformity were achieved (~1 h). The slurry was cast on battery-grade aluminum foil using a doctor blade (MTI corp) with a thickness of 30–120 μm . Once cast, the slurry was kept under a closed fume hood for 2 h before transferring to a vacuum oven, where it was dried at 50°C for 24 h.

2.3. Characterization

2.3.1. Material characterization

Morphological analysis of the materials was conducted using an SEM (Zeiss Supra 50VP, Germany) with an in-lens detector. A30 mm aperture was used to examine the morphology and obtain micrographs of the samples. To analyze the surface elemental composition, EDS (Oxford Instruments) in secondary electron detection mode was used. To analyze the sulfur deposition on the surface, TEM measurements were conducted. Highresolution transmission electron microscope, HRTEM, analyses were performed in a bright field mode operated at 200 kV on a JEOL JEM2100F equipped with an EDS, with an 80 mm² SSD detector (Oxford X-MaxN 80 T EDS system). XRD patterns were acquired on a diffractometer (Rigaku Miniflex, Tokyo, Japan) using Cu Ka radiation (40 kV and 40 mA) with a step size of 0.02° and dwell time of 5 s, in the $2^{\circ}-65^{\circ}$ 2θ range. The surface of the composites was analyzed with XPS. To collect XPS spectra, Al-Ka X-rays with a spot size of 200 mm and pass energy of 23.5 eV were used to irradiate the sample surface. A step size of 0.05 eV was used to gather the high-resolution spectra. CasaXPS Version 23.19PR1.0 software was used for spectra analysis. The sulfur in the composite was determined using TGA on a TA Instruments Q50. The samples were heated at a ramp rate of 10°C·min⁻¹ to 800°C under flowing argon gas.

2.3.2. Electrochemical characterization

2.3.2.1. Coin cell fabrication. The dried electrodes were cut using a hole punch ($\phi = 1/2$ inch [12.72 mm]) to form disk-sized electrodes. The electrodes were then weighed and transferred to an argonfilled glove box (MBraun Lab star, O₂ < 1 ppm, and $H_2O < 1$ ppm). The CR2032 (MTI Corporation and Xiamen TMAX Battery Equipment) coin-type Li-S cells were assembled using DMX/S ($\phi = 12$ mm), lithium disk anodes (Xiamen TMAX Battery Equipment's; [$\phi = 15.6 \text{ mm}$ and 450 μm thick]), a trilayer separator (Celgard 2325; $\varphi = 19$ mm), and one SS spring and two spacers along with an electrolyte. The electrolytes, 1 M LiPF₆ in EC:DEC (1:1), 1 M NaPF₆ in EC:PC (1:1) with 5% fluoroethylene carbonate (FEC), and 1 M KPF₆ in EC: DEC (1:1), were made after predrying the solvent with molecular sieves. The assembled coin cells were rested at their open-circuit potential for 12 h to equilibrate them before performing electrochemical experiments at RT. Cyclic voltammetry (CV) was performed at various scan rates (0.1 mV/s to 0.5 mV/s) between voltages 0.1 and 3 V wrt Li/Li⁺, Na/Na⁺, and K/K⁺ were performed using a potentiostat (Biologic VMP3). Prolonged cyclic stability tests were carried out with a MACCOR (4000 series) and Neware BTS 4000 battery cycler at different C-rates (where 1 C = 1,675 mAh/g) between voltages 0.1 and 3.0 V. All cells were conditioned during the first cycle at the 0.1 C and second cycle at 0.2 C rate before cycling them at the 0.5 C rate at room temperature.

3. Results and discussion

To synthesize our cathodes, we first treated ML MXenes with DHT and used them as host materials because of their high interlayer spacing for enhanced S intercalation. The mixture of DHT-treated MXenes, DMX, and S was subjected to thermal treatment at 350°C for S intercalation into the interlayer spacings as described in the experimental section. Scanning electron microscope (SEM) images show the composites retain the ML structure with no aggregates before (Fig. 2a) or after thermal treatment (Fig. 2b). As a reference, we also thermally treated DMX (without sulfur), and it also shows a similar ML structure (supp. Fig. 1), suggesting thermal treatment does not affect it. Elemental mapping using EDS further shows the presence of uniformly distributed S in the composite (supp. Fig. 2).

Fig. 2c and d shows XRD patterns of the DMX, DMX/S, and heattreated DMX powders. The XRD pattern of DMX/S shows peaks pertaining to MXenes with no evidence of crystalline S. The absence of crystalline peaks of octa-sulfur suggests it is present in an amorphous state. The 2θ peak corresponding to (002) plane represents the interlayer spacing between the MXene sheets. After

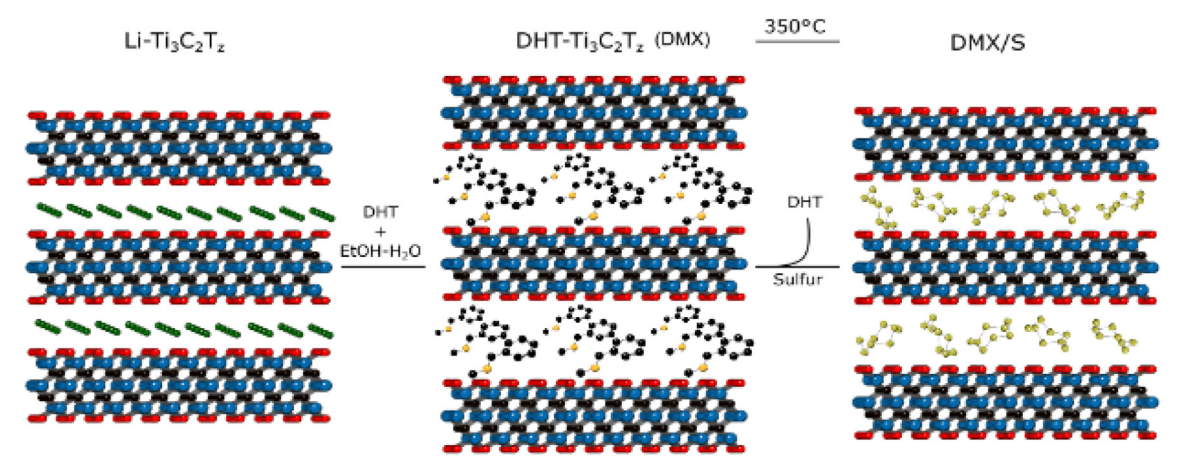


Fig. 1. Schematic illustration of fabrication procedure for DMX/S powders.

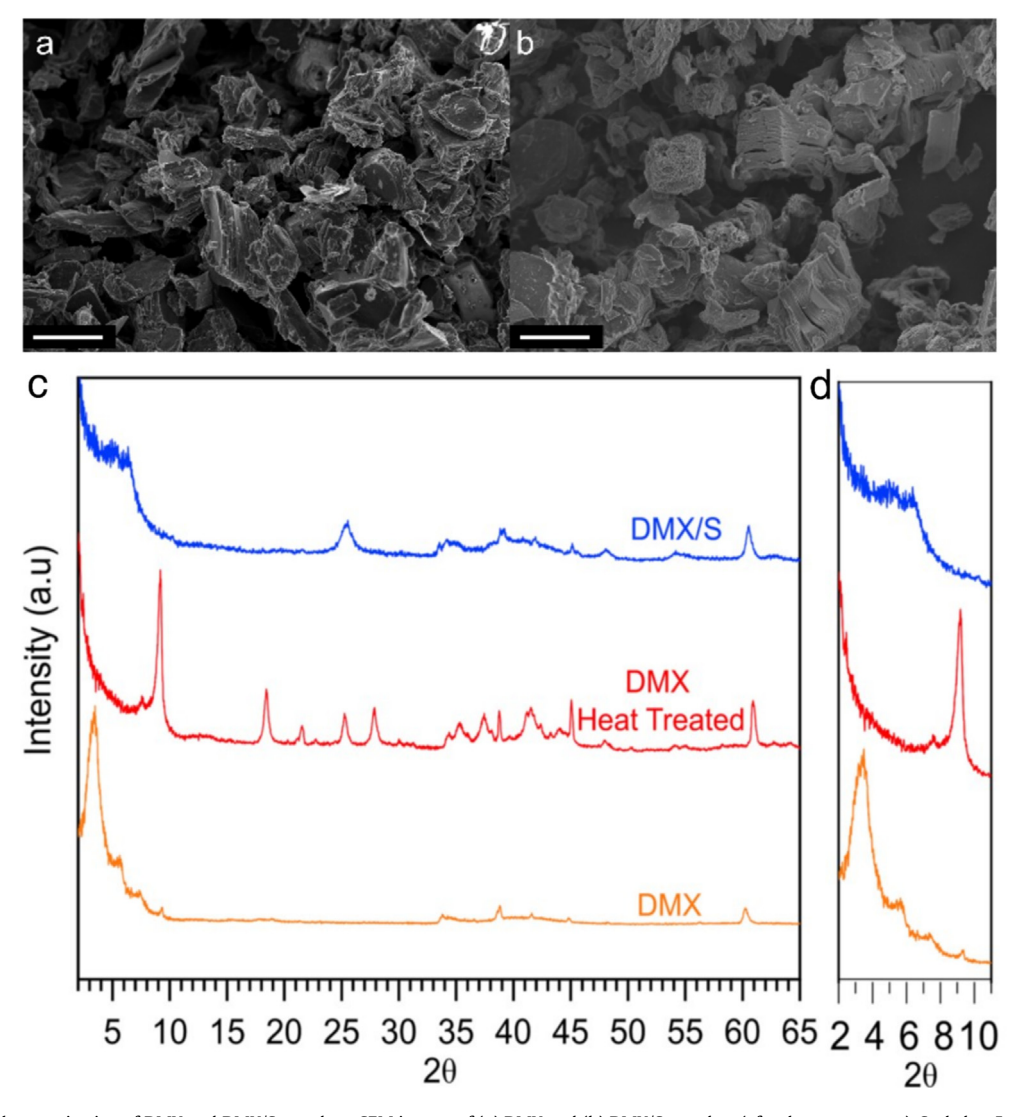


Fig. 2. Morphological characterization of DMX and DMX/S powders: SEM images of (a) DMX and (b) DMX/S powders (after heat treatment). Scale bar 5 μm. XRD diffraction of (c) DMX (orange, bottom), DMX/S after heat treatment (red, middle), and DMX/S (blue, top) powders, (d) is same as "c" but only focused on the 2–10 2θ range.

thermal treatment in DMX/S, the intensity of that peak reduces substantially and broadens as seen in the zoomed-in XRD (2–10° 2θ) in Fig. 2d. The center of the peak also shifts from about 3.9° to about 6.1° 2θ , which corresponds to a reduction of interlayer spacing from 2.3 nm to 1.4 nm. The reduction in interlayer spacing suggests probable degradation of the DHT molecules, leading to a decrease in interlayer spacing. Interestingly, the 002 peak shifts to 9.18° 2θ for heat-treated DMX without sulfur, suggesting a significant decrease in interlayer spacing (0.9 nm). Comparing the d-spacing values of all three powders suggests sulfur species mitigate the further collapse of the interlayer spacing in DMX powders with heat treatment suggesting the intercalation of sulfur species in between the DMX sheets.

To get a deeper understanding of the S confinement in between the MXene sheets, TEM and its corresponding EFTEM experiments were conducted on DMX/S flakes. Typical TEM images of a flake show an ML structure as shown in Supp. Fig. 3a. Occasionally, small aggregates on the surface resulting from the oxidation of some MXene flakes to TiO₂ are observed. The selected area electron diffraction (SAED) pattern in Supp. Fig. 3b corresponds to the hexagonal pattern of MXenes. Diffused rings, corresponding to

polycrystalline S, were not observed in the SAED pattern possibly because of their confinement in between the MLs. Nevertheless, the EDS spectra (Supp. Fig. 3c) show the presence of S. EFTEM images acquired from a thin and uniform region (Supp. Fig. 3d) further corroborate the presence of S (Supp. Fig. 3f), which is uniformly distributed across the DMX/S flake along with Ti (Supp. Fig. 3e).

Supplementary Fig. 4 shows the XPS spectra of MXene without (a—c) and with S after thermal treatment (d—f). The C1s spectra in both samples show the existence of the Ti—C—Ti MXene peaks in addition to surface adventitious C and C bonded to O at binding energies, BEs, 281.6, 284.6, and 286.8 eV, respectively [22]. There is ~0.7 eV shift in the C-Ti-Tz peak in the C 1s spectra after sulfur intercalation because of possible interactions of sulfur atoms with the surface titanium atoms causing some shift in the electron density in the C-Ti bonds. The O1s spectra show the presence of TiO2 species, which is possibly because of surface oxidation during heat treatment. As expected, the high-resolution XPS spectra in the S2p region exhibit a doublet S2p3/2 and S2p1/2 in the MXene/S composite at BEs of 161.8 eV and 163.7 eV with an intensity ratio of 0.51 indicating the presence of S.

R. Pai, V. Natu, M. Sokol et al.

Materials Today Energy 27 (2022) 101000

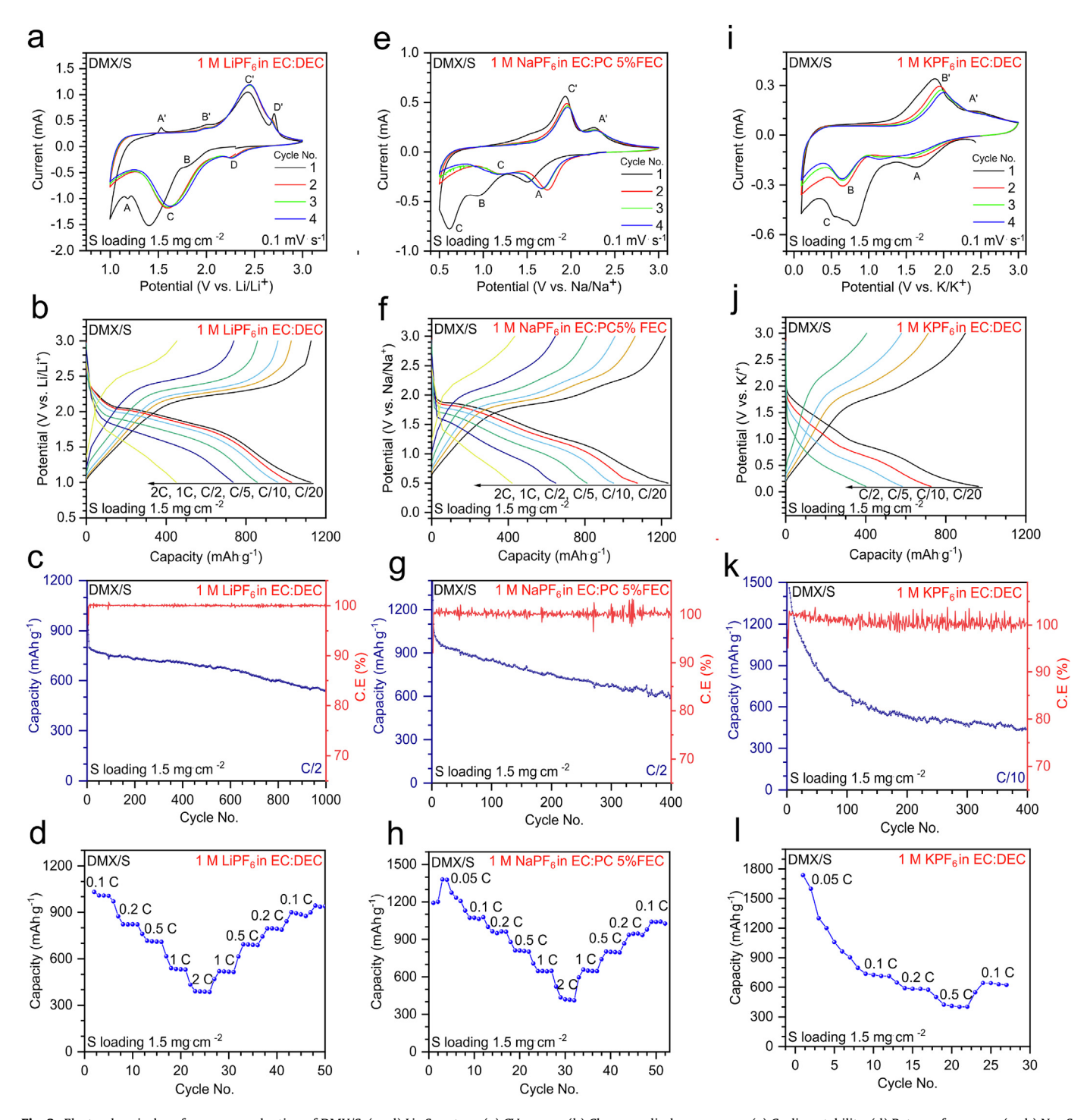


Fig. 3. Electrochemical performance evaluation of DMX/S. (a–d) Li–S system. (a) CV curves, (b) Charge – discharge curves, (c) Cycling stability, (d) Rate performance, (e–h) Na–S system, (e) CV curves, (f) Charge – discharge curves, (g) Cycling stability, (h) Rate performance. (i–l) K–S system, (i) CV curves, (j) Charge – discharge curves, (k) Cycling stability, (l) Rate performance. In c, g and k, the right y-axis is couloumbic efficiency.

The DMX/S composite contains around 25 wt% S in the composite as determined by TGA (Supp. Fig. 5). The TGA curves show two weight loss zones, one from 100 to 200°C and another from 200 to 350°C. The first zone is most probably associated with S loss from the edges of the MXene sheets and in large pores; the latter from between the MXene layers themselves [39]. The enhanced thermal stability of the confined S can be attributed to its strong confinement and interaction with the MXenes sheets.

To test the electrochemical response of our DMX/S system, coin cells were assembled with DMX/S as the cathode and Li, Na, or K foils as anodes. The electrolyte in the Li, Na, and K case was 1 M LiPF₆, 1 M NaPF₆ (EC:PC), and 1 M KPF₆, respectively in EC:DEC. In the Na system, 5 vol% FEC was added to the electrolyte. Fig. 3 presents typical CV curves, galvanostatic charge—discharge curves, and cycling tests of DMX/S cathodes in Li, Na, and K systems. The first CV curve in the Li—S cell demonstrates three

reduction and oxidation peaks in 1–3 V potential window vs. Li/Li⁺. The redox pair A-A' is observed only in the first cycle and can possibly be because of the irreversible redox behavior between the MXene nanosheets and the carbonate electrolyte (Fig. 3a). The redox pairs B-B' and D-D' are possibly because of intercalation and the pseudocapacitive behavior of MXene in organic electrolytes, respectively, as noted in previous reports [40,41]. The redox pair B-B' is also present in the thermally treated DMX cathode (without S) as shown in Supp. Fig. 6a. Nevertheless, the capacity contribution from the B-B' and D-D' peaks is negligible and only present for the first 20 cycles (Supp. Fig. 7). After 10 cycles, the single redox pair C-C'—corresponds to the conversion of S₈ to Li₂S via a solid-state conversion, possibly because of the desolvation of Li ions, which dominates the charge transfer reaction [16,42]. We believe the interlayer distance of MXene nanosheets after thermal treatment facilitates Li-ion desolvation leading to a quasi-solid-state conversion. This possibly enables the intermediate polysulfides to remain within the stacked interlayers preventing contact and consequently adverse reactions with the carbonate solvent [18,43]. A single broad peak in oxidation and reduction reactions is possibly an effect of a lower energy barrier for polysulfides to Li₂S conversion. Normal MXenes without DHT treatment subjected to sulfur deposition technique did not contribute to significant current response (Supp. Fig. 8). This suggests a requirement of higher initial interlayer spacing for sulfur intercalation, which the DMX host provides, which reduces after thermal treatment, confining sulfur in between the sheets as depicted by the diffraction pattern in Fig. 3. The charge—discharge plateaus are consistent with the CV curves showing only a single plateau, unlike conventional ether-based Li—S redox reactions that show two plateaus.

The DMX/S electrode demonstrates a high discharge capacity of 1,100 mAh/g at a C/10 rate in Li-S batteries. To estimate the capacity originating from the DMX host alone, we performed the same charge—discharge tests at the same current per gram of active material (~20 mA/g) as for the S composite, and the capacity was only ~35 mAh/g (Supp. Fig. 6b). It is clear that the host material does not contribute much to the capacity, and it is indeed the S that is playing the dominant role. The long-term cycling was performed at C/2 rate and the DMX/S delivered 750 mAh/g (capacity retention = ~94%), 733 mAh/g (92%), 688 (86%), and 550 mAh/g (69%) after 100, 200, 500, and 1,000 cycles, respectively. The cells were rested for 12 h and conditioned at C/10 and C/5 for two cycles each. The cathode delivered an average Coulombic efficiency of 99.98% over 1,000 cycles indicating complete utilization of S with negligible side and/or polysulfide reactions with the carbonate species. To further understand the cathode's behavior under various currents, rate analyses were performed. Such tests shed light on the mass diffusion of Li⁺ in the interlayer spacing. The DMX/S cathode delivered a capacity of 1,050, 830, 730, 550, and 400 mAh/g at C/10, C/5, C/2, 1C, and 2C, respectively (Fig. 3d). Furthermore, when the current was decreased back to C/5 and C/10, the capacities rebounded to 800 and 950 mAh/g, respectively, demonstrating the robustness of the cathode toward electrochemical stresses.

The DMX/S cathodes were also cycled with a Na anode (Fig. 3e). The potential window was increased for complete conversion of the reduction peak. Although Li-/Na-S cells both have multistep redox reactions, the large size and poor mobility of Na-ions complicate the electrochemical reactions of the Na-S cells. The sluggish reaction kinetics cause high polarization that the operating voltage window, in turn, shifts toward lower discharge voltages of ≈ 0.5 V [44]. The first reduction cycle shows three reduction peaks. We attribute the first peak at ~ 1.5 V (A) to the reduction of S to Na₂S_x; the second at ~ 0.9 V (B) to the decomposition of electrolyte and subsequent solid electrolyte interphase (SEI) formation and the

third peak, at ~ 0.6 V (C), to further reduction of Na₂S_x (x = 4–8) to Na₂S₂ and Na₂S [45-47]. In subsequent cycles, we see only two reduction peaks (A-A' and C-C') that can be associated with the formation of S to Na_2S_x followed by Na_2S_x to Na_2S_2 and Na_2S . We also observe a lower polarization gap during reduction cycles for similar conversions. For the first time, compared with prior literature, we observe two dominant and repeatable redox pairs in the Na-S system with carbonate electrolyte. The two redox peaks demonstrated by the DMX/S cathode coupled with a Na anode show a striking difference compared with its use with Li anodes. Usually, a single pair of redox peaks are reported in the literature and are associated with the conversion of small S molecules (S2-S4) to Na₂S. However, here, we believe S exists in its octa-sulfur polymorph (S₈) because of the relatively lower synthesis temperature and the higher interlayer spacing (2.2 nm compared with <0.7 nm for microporous carbon) within the ML-DMX sheets is enabling successful intercalation/confinement of larger S₈ molecules. Traditionally, Na₂S_x is formed at ~2.2 V; however, in our work, the peak is seen at ~1.7 V (~1.5 V in the first cycle), which could be attributed to the additional energy barrier needed for Na-ions to strip out of their solvation shell (>1.8 nm) and diffuse into the narrow interlayer spacing of the DMX sheets [9]. A lower peak voltage in the first cycle may be associated with the formation of an ionconductive SEI, alleviating the energy required for Na-ions to intercalate into the DMX host [47]. In the oxidation cycle, again, we observe two peaks related to the conversion of Na₂S to Na₂S_x and Na₂S_x to S₈. As discussed earlier, the successful repeatable operation in carbonate electrolyte suggests that the Na₂S_x formed does not come in contact with the electrolyte because of its confinement both within the MXene sheets and SEI layer.

To understand the electrochemical behavior of thermally treated DMX cathodes (without S) as a reference (Supp. Fig. 6c), they were cycled in the same electrolyte. A single reduction peak was observed at 0.9 V vs Na/Na⁺ in the first cycle (also seen in the first cycle of DMX/S), which is associated with the formation of SEI, after which the electrode delivers a double-layer capacitance. Comparing the CV curves of DMX/S and DMX shows the existence of two additional redox peaks only in the DMX/S host, confirming their origin from S redox.

To further evaluate the electrochemical performance, galvanostatic charge-discharge tests were performed. charge-discharge plateaus exhibit a similar trend as seen in CV curves (Fig. 3f). The DMX/S powders deliver an initial capacity of 1,400 mAh/g at C/20, which is attributed to S₈ reduction to Na₂S and solvent decomposition resulting in SEI formation. A 1,100 mAh/g capacity is retained after the first cycle. It is worth noting that the irreversible capacity loss possibly because of SEI formation in the first cycle is relatively small and accounts for ~300 mAh/g, which can be associated with the low surface area of our ML MXene sheets. The capacity stabilizes at 900 mAh/g after the first few cycles and delivers a capacity of 850 mAh/g (capacity retention = \sim 94.4%), 730 mAh/g (81%), 650 mAh/g (72.2%), and ~600 mAh/g (~67% capacity retention) after 100, 200, 300, and 400 cycles, respectively, at C/2 (Fig. 3g). The rate performance in Fig. 3h was evaluated at C/10, C/5, C/2, 1C, and 2C wherein the cathode delivered capacities of 1050, 950, 800, 600, and 400 mAh/g, respectively. On reducing the current to C/10, a capacity of 1,000 mAh/g was recovered. The high capacity retention, at various current rates, can be attributed to the host conductivity and ion transport.

The electrochemical performance of DMX/S cathodes was further evaluated with K anodes. The DMX/S cathodes were cycled from 0.1 to 3.0 V wrt K/K^+ in carbonate electrolyte. Fig. 3i shows the CV curves of DMX/S in the K-S system. The anodic curves show two reduction peaks at 1.7 V (A) and a broad

convoluted hump from 1.1 to 0.4 V (B & C) wrt K/K⁺. Based on our initial hypothesis on confinement of S₈ in the layered structure and desolvation of K⁺ ions resulting in the reduction of the species, the first reduction peak can be attributed to the conversion of S₈ to K₂S_X [48]. The broad hump probably is a combination of two peaks resulting from the reduction of electrolyte on the electrode surface, C (~0.9 V wrt $\mbox{K}/\mbox{K}^{+})$ and reduction of $\mbox{K}_{2}\mbox{S}_{X}$ to K_2S_3 , K_2S_2 , and K_2S , B (~0.7 V wrt K/K⁺) [10]. Compared with Li-S and Na-S systems, we need to shift the voltages of the K-S system to the lower end (0.1 V) to observe the complete conversion of the reaction because of its sluggish kinetics. In subsequent cycles, we observe only two sharp reduction peaks related to S₈ reduction at 1.6 V and 0.7 V wrt K/K⁺. During the oxidation cycle, we observe two peaks at 2 V and 2.5 V wrt K/K⁺ demonstrating the conversion of solid K₂S to K₂S_X and K₂S_X to S₈, respectively. Xiong et al. reported infusion of small S molecules in microporous carbon with high-temperature treatment (~600°C) and observed two reduction peaks positioned at 1.5 and 0.85 V wrt K/K⁺. However, the scan rate used in the literature is low (0.01 mV/s) compared with this study (0.1 mV/s), which can explain the peak shifts [48]. Interestingly, they observed two peaks similar to the present study despite the presence of small S molecules as the active material. We believe the SEI layer formed in the first cycle prevents the interaction of the electrolyte with the S species and consequently any adverse reactions. Also, similar to the Na-S system, the increased polarization gap in between redox reactions results in the observation of two peaks in the K-S system compared with a single peak in Li-S. The charge-discharge plateaus obey similar patterns as the CV curves. The cathode delivers an initial capacity of ~1,700 mAh/g at C/20, which is higher than the theoretical capacity of S₈, denoting some capacity is originating from the reduction of S_8 as well as the irreversible reduction of the electrolyte (SEI) in the first cycle. The capacity then reduces at ~1,400 mAh/g in subsequent cycles, which is expected to be fully attributable to the S₈ reduction reaction. The cathode delivers a capacity of 700 mAh/g, 500 mAh/g, 450 mAh/g, and 400 mAh/g after 100, 200, 300, and 400 cycles, respectively, at a C/10 current rate. The rapid decrease in capacity can be attributed to the larger K⁺ ions (0.276 nm) rupturing the SEI layer and eliminating the confinement effect. However, further study needs to be carried out to understand this effect completely. Because of sluggish kinetics, the rate capability was performed at C/20, C/10, C/5, and C/2 as shown in Fig. 3i, wherein the cathode delivered a capacity of 900, 700, 600, and 400 mAh/g, respectively. For comparison, we cycled the thermally treated DMX (without S) in the similar voltage range with similar gravimetric current densities (Supp. Fig. 6 e,f). A single reduction peak in the 1st cycle is attributed to SEI formation and is also observed for DMX/S cathode, after which the electrode delivers a double-layer capacitance in subsequent cycles. During the charge-discharge tests the capacity contribution is higher compared with Li-S and Na-S system because of the lower current density in K-S system.

4. Conclusion

In conclusion, for the first time, we demonstrate the utilization of highly conductive MXene sheets as a confinement source for S_8 molecules enabling solid-state conversion in carbonate electrolytes in alkali metal (Li/Na/K)-S systems. Compared with conventional liquid phase Li-S electrochemical reactions, this quasi-solid-state mechanism has various advantages, which can provide a new paradigm for future metal-S battery materials design and synthesis. Our findings provide a universal host to fabricate high-performance

room-temperature alkali metal—S batteries using carbonate electrolyte, a more commercially viable choice.

Authors' contribution

R.P. contributed to conceptualization, writing the original draft preparation, and investigation. V.N. contributed to conceptualization and reviewing and editing the article. M.C. and M.S. contributed to resources. T.G. contributed to industry perspective and funding acquisition. M.B. contributed to supervision, reviewing and editing, and funding acquisition. V.K. contributed to supervision, reviewing and editing the article, and funding acquisition.

Declaration of competing interest

The authors declare that they have no known competing financial interests or personal relationships that could have appeared to influence the work reported in this paper.

Acknowledgments

The authors are especially thankful to the MCC facility at Drexel University for help with materials characterization equipment. The authors would also like to thank Dr. Giuseppe Palmese's group for their help with thermogravimetric analysis. The authors would also like to thank the National Science Foundation (DMR-1740795 and CMMI - 1919177) for funding this work.

Appendix A. Supplementary data

Supplementary data to this article can be found online at https://doi.org/10.1016/j.mtener.2022.101000.

References

- A.K. Padhi, K.S. Nanjundaswamy, J.B. Goodenough, Phospho-olivines as positive-electrode materials for rechargeable lithium batteries, J. Electrochem. Soc 144 (1997) 1188–1194.
- [2] M. Li, J. Lu, Z. Chen, K. Amine, 30 Years of lithium-ion batteries, Adv. Mater. 30 (2018) 1800561.
- [3] P.G. Bruce, S.A. Freunberger, L.J. Hardwick, J.M. Tarascon, Li-O2 and Li-S batteries with high energy storage, Nat. Mater. 11 (2011) 19–29.
- [4] A. Manthiram, Y. Fu, S.H. Chung, C. Zu, Y.S. Su, Rechargeable lithium-sulfur batteries, Chem. Rev. 114 (2014) 11751–11787.
- [5] S.H. Chung, A. Manthiram, Current status and future prospects of metal-sulfur batteries, Adv. Mater. 31 (2019) 1901125.
- [6] M. Wild, L. O'Neill, T. Zhang, R. Purkayastha, G. Minton, M. Marinescu, G.J. Offer, Lithium sulfur batteries, a mechanistic review, Energy Environ. Sci. 8 (2015) 3477–3494.
- [7] Y.X. Yin, S. Xin, Y.G. Guo, L.J. Wan, Lithium-sulfur batteries: electrochemistry, materials, and prospects, Angew. Chem., Int. Ed. Engl. 52 (2013) 13186–13200.
- [8] S. Xin, Y.X. Yin, Y.G. Guo, L.J. Wan, A high-energy room-temperature sodiumsulfur battery, Adv. Mater. 26 (2014) 1261–1265.
- [9] S. Wei, S. Xu, A. Agrawral, S. Choudhury, Y. Lu, Z. Tu, L. Ma, L.A. Archer, A stable room-temperature sodium-sulfur battery, Nat. Commun. 7 (2016) 11722.
- [10] J. Ding, H. Zhang, W. Fan, C. Zhong, W. Hu, D. Mitlin, Review of emerging potassium-sulfur batteries, Adv. Mater. 32 (2020) 1908007.
- [11] L. Wang, Y. Ye, N. Chen, Y. Huang, L. Li, F. Wu, R. Chen, Development and challenges of functional electrolytes for high-performance lithium-sulfur batteries, Adv. Funct. Mater. 28 (2018).
- [12] B. Flamme, G. Rodriguez Garcia, M. Weil, M. Haddad, P. Phansavath, V. Ratovelomanana-Vidal, A. Chagnes, Guidelines to design organic electrolytes for lithium-ion batteries: environmental impact, physicochemical and electrochemical properties, Green Chem. 19 (2017) 1828—1849.
- [13] T. Cleaver, P. Kovacik, M. Marinescu, T. Zhang, G. Offer, Perspective—commercializing lithium sulfur batteries: are we doing the right research? J. Electrochem. Soc. 165 (2017) A6029—A6033.
- [14] S.S. Zhang, Liquid electrolyte lithium/sulfur battery: fundamental chemistry, problems, and solutions, J. Power Sources 231 (2013) 153–162.
- [15] T. Yim, M.-S. Park, J.-S. Yu, K.J. Kim, K.Y. Im, J.-H. Kim, G. Jeong, Y.N. Jo, S.-G. Woo, K.S. Kang, I. Lee, Y.-J. Kim, Effect of chemical reactivity of polysulfide

- toward carbonate-based electrolyte on the electrochemical performance of Li–S batteries, Electrochim. Acta 107 (2013) 454–460.
- [16] M. Helen, T. Diemant, S. Schindler, R.J. Behm, M. Danzer, U. Kaiser, M. Fichtner, M. Anji Reddy, Insight into sulfur confined in ultramicroporous carbon, ACS Omega 3 (2018) 11290—11299.
- [17] H. Maria Joseph, M. Fichtner, A.R. Munnangi, Perspective on ultramicroporous carbon as sulphur host for Li—S batteries, J. Energy Chem. 59 (2021) 242—256.
- [18] E. Markevich, G. Salitra, Y. Talyosef, F. Chesneau, D. Aurbach, Review—on the mechanism of quasi-solid-state lithiation of sulfur encapsulated in microporous carbons: is the existence of small sulfur molecules necessary? I. Electrochem. Soc. 164 (2016) A6244—A6253.
- [19] M. Naguib, M. Kurtoglu, V. Presser, J. Lu, J. Niu, M. Heon, L. Hultman, Y. Gogotsi, M.W. Barsoum, Two-dimensional nanocrystals produced by exfoliation of Ti3AlC2. Adv. Mater. 23 (2011) 4248–4253.
- [20] L. Verger, V. Natu, M. Carey, M.W. Barsoum, MXenes: an introduction of their synthesis, select properties, and applications, Trends Chem 1 (2019) 656–669.
- [21] M. Sokol, V. Natu, S. Kota, M.W. Barsoum, On the chemical diversity of the MAX phases, Trends Chem 1 (2019) 210–223.
- [22] M. Carey, Z. Hinton, V. Natu, R. Pai, M. Sokol, N.J. Alvarez, V. Kalra, M.W. Barsoum, Dispersion and stabilization of alkylated 2D MXene in nonpolar solvents and their pseudocapacitive behavior, Cell Rep. Phys. Sci. 1 (2020) 100042
- [23] K. Hantanasirisakul, M.-Q. Zhao, P. Urbankowski, J. Halim, B. Anasori, S. Kota, C.E. Ren, M.W. Barsoum, Y. Gogotsi, Fabrication of Ti3C2TxMXene transparent thin films with tunable optoelectronic properties, Adv. Electron. Mat. 2 (2016) 1600050.
- [24] M. Ghidiu, M.R. Lukatskaya, M.Q. Zhao, Y. Gogotsi, M.W. Barsoum, Conductive two-dimensional titanium carbide 'clay' with high volumetric capacitance, Nature 516 (2014) 78–81.
- [25] B. Anasori, M.R. Lukatskaya, Y. Gogotsi, 2D metal carbides and nitrides (MXenes) for energy storage, Nat. Rev. Mater. 2 (2017) 16098.
- [26] A.D. Dillon, M.J. Ghidiu, A.L. Krick, J. Griggs, S.J. May, Y. Gogotsi, M.W. Barsoum, A.T. Fafarman, Highly conductive optical quality solution-processed films of 2D titanium carbide, Adv. Funct. Mater. 26 (2016) 4162–4168.
- [27] K. Hantanasirisakul, Y. Gogotsi, Electronic and optical properties of 2D transition metal carbides and nitrides (MXenes), Adv. Mater. 30 (2018) 1804779.
- [28] V. Kamysbayev, A.S. Filatov, H. Hu, X. Rui, F. Lagunas, D. Wang, R.F. Klie, D.V. Talapin, Covalent surface modifications and superconductivity of twodimensional metal carbide MXenes, Science 369 (2020) 979–983.
- [29] D. Han, J. Zhang, Z. Weng, D. Kong, Y. Tao, F. Ding, D. Ruan, Q.-H. Yang, Two-dimensional materials for lithium/sodium-ion capacitors, Mater, Today Energy 11 (2019) 30–45.
- [30] A.S. Etman, J. Halim, J. Rosen, Mo1.33CTz—Ti3C2Tz mixed MXene freestanding films for zinc-ion hybrid supercapacitors, Mater, Today Energy 22 (2021)
- [31] M. Ghidiu, J. Halim, S. Kota, D. Bish, Y. Gogotsi, M.W. Barsoum, Ion-exchange and cation solvation reactions in Ti3C2MXene, Chem. Mater. 28 (2016) 3507–3514.
- [32] M.-C. Liu, B.-M. Zhang, Y.-S. Zhang, B.-N. Gu, C.-Y. Tian, D.-T. Zhang, Y.-Q. Wang, B. Zhao, Y.-Y. Wang, M.-J. Liu, Y.-J. Yu, K. Zhao, L.-B. Kong, Y.-L. Chueh, Regulating interlayer spacing with pillar and strain structures in Ti3C2 MXene layers by molecular welding for superior alkali metal ion storage, Mater. Today Energy 22 (2021) 100832.
- [33] T. Ruan, B. Wang, Q. Lv, Y. Jiang, D. Wang, Interface coupling in FeOOH/MXene heterojunction for highly reversible lithium-ion storage, Mater. Today Energy 19 (2021) 100584.
- [34] Q. Zhao, Q. Zhu, Y. Liu, B. Xu, Status and prospects of MXene-based lithium—sulfur batteries, Adv. Funct. Mater. 31 (2021) 2100457.
- [35] R. Pai, V. Natu, M. Sokol, M. Carey, M.W. Barsoum, V. Kalra, Tuning functional two-dimensional MXene nanosheets to enable efficient sulfur utilization in lithium-sulfur batteries, Cell Reports Physical Science 2 (2021) 100480.
- [36] K.B. Hueso, M. Armand, T. Rojo, High temperature sodium batteries: status, challenges and future trends, Energy Environ. Sci. 6 (2013) 734–749.
- [37] D. Kumar, S.K. Rajouria, S.B. Kuhar, D.K. Kanchan, Progress and prospects of sodium-sulfur batteries: a review, Solid State Ionics 312 (2017) 8–16.
- [38] X. Zhao, Y. Lu, Z. Qian, R. Wang, Z. Guo, Potassium-sulfur batteries: status and perspectives, EcoMat 2 (2020) 12038.
- [39] M. Xue, C. Chen, Y. Tan, Z. Ren, B. Li, C. Zhang, Mangosteen peel-derived porous carbon: synthesis and its application in the sulfur cathode for lithium sulfur battery, J. Mater. Sci. 53 (2018) 11062–11077.
- [40] M. Naguib, J. Come, B. Dyatkin, V. Presser, P.-L. Taberna, P. Simon, M.W. Barsoum, Y. Gogotsi, MXene: a promising transition metal carbide anode for lithium-ion batteries, Electrochem. Commun. 16 (2012) 61–64.
- [41] N. Kurra, M. Alhabeb, K. Maleski, C.-H. Wang, H.N. Alshareef, Y. Gogotsi, Bistacked titanium carbide (MXene) anodes for hybrid sodium-ion capacitors, ACS Energy Lett. 3 (2018) 2094—2100.
- [42] C. Fu, B.M. Wong, K.N. Bozhilov, J. Guo, Solid state lithiation-delithiation of sulphur in sub-nano confinement: a new concept for designing lithiumsulphur batteries, Chem. Sci. 7 (2016) 1224–1232.

- [43] S. Xin, L. Gu, N.H. Zhao, Y.X. Yin, L.J. Zhou, Y.G. Guo, L.J. Wan, Smaller sulfur molecules promise better lithium-sulfur batteries, J. Am. Chem. Soc. 134 (2012) 18510–18513.
- [44] Z. Yan, Y. Liang, J. Xiao, W. Lai, W. Wang, Q. Xia, Y. Wang, Q. Gu, H. Lu, S.L. Chou, Y. Liu, H. Liu, S.X. Dou, A high-kinetics sulfur cathode with a highly efficient mechanism for superior room-temperature Na-S batteries, Adv. Mater. 32 (2020) 1906700.
- [45] S. Kajiyama, L. Szabova, K. Sodeyama, H. Iinuma, R. Morita, K. Gotoh, Y. Tateyama, M. Okubo, A. Yamada, Sodium-ion intercalation mechanism in MXene nanosheets, ACS Nano 10 (2016) 3334–3341.
- [46] X.B. Cheng, R. Zhang, C.Z. Zhao, F. Wei, J.G. Zhang, Q. Zhang, A review of solid electrolyte interphases on lithium metal anode, Adv. Sci. 3 (2016) 1500213.
- [47] J. Lee, J. Kim, S. Kim, C. Jo, J. Lee, A review on recent approaches for designing the SEI layer on sodium metal anodes, Mater. Adv. 1 (2020) 3143–3166.
- [48] P. Xiong, X. Han, X. Zhao, P. Bai, Y. Liu, J. Sun, Y. Xu, Room-temperature potassium-sulfur batteries enabled by microporous carbon stabilized smallmolecule sulfur cathodes, ACS Nano 13 (2019) 2536–2543.



Rahul Pai is a Ph.D. candidate in the Department of Chemical and Biological Engineering at Drexel University and is currently interning at Tesla. He received his master's degree in the Chemical and Biological Engineering from Drexel University in 2017 and Bachelors of Engineering from University of Mumbai in 2015. His research focuses on the development of materials for energy storage devices.



Varun Natu is a Ph.D. candidate in the Department of Materials science and engineering at Drexel University. He has received his Bachelor of Engineering from NBN Sinhgad School of Engineering, Pune. His research focuses on synthesis and development of novel 2D transition metal carbides and nitrides (MXenes) and understanding the surface properties of these materials.



Dr. Maxim Sokol is a Senior Lecturer in the Department of Materials Science and Engineering at Tel-Aviv University and head of the Advanced Ceramics Laboratory. The laboratory focuses on the development of novel nanostructured ceramics, ceramic nanocomposites, atomically laminated metal-ceramic compounds such as MAX and MAB phases, synthesis of two-dimensional transition metal carbides, and nitrides known as MXene, high-temperature behavior of materials and advanced sintering methods. Sokol earned a B.Sc. in Physics, a B.Sc., M.Sc., and a Ph.D. in Materials Engineering from Ben-Gurion University of the Negev, Beer-Sheva, Israel. After receiving his Ph.D., Sokol joined the Department of Materials Science and Engineering at Drexel University as a postdoctoral researcher where he worked on diverse projects related to MXenes-enabled applications and processes in Prof. Barsoum's Layered Solids Laboratory. As a postdoctoral researcher, Sokol was awarded The Louis and Bessie Stein Family Fellowship.



Thomas Greszler manages the Li-Ion development team for Saft in Cockeysville, MD focusing on industrialization/ scale-up of advanced battery concepts along with R&D on battery materials including ultra-high-power cells, lithium-titanate, advanced phosphate cells and solid-state. He joined Saft in 2013. Previously, from 2005 until 2013, he worked for General Motors developing fuel cell catalysts and electrodes while leading the GM Electrochemical Cell Design group which provided fuel cell and battery cell modeling to support system design, cost trade-offs, fundamental understanding and improved performance/ durability. He has written seven technical papers, one book chapter, has ten patents pending/issued, and has presented results at many technical conferences. Education includes a BS in 2003 and MS in 2005 both in Chemical Engineering from Case Western Reserve University and a MBA from the University of Rochester in



Prof. Michel W. Barsoum is a Distinguished Professor in the Department of Materials Science and Engineering at Drexel University. He is an internationally recognized leader in the area of MAX phases, and more recently, the 2D solids labeled MXenes derived from the MAX phases. Most recently he also discovered a new universal mechanism — ripplocation - in the deformation of layered solids. With over 500 refereed publications and a Google h index

is 119, his work has been highly and widely cited. He was on the Web of Science's highly cited researchers list in 2018, 2019, and 2020. In 2020, according to a recent Stanford University study, he had the highest c-index (combines citations and h-index) in the Materials Science subfield. He is a foreign member of the Royal Swedish Society of Engineering Sciences, a fellow of the American Ceramic Soc., and the World Academy of Ceramics. He is the author of the books, MAX Phases: Properties of Machinable Carbides and Nitrides and Fundamentals of Ceramics, a leading textbook in his field. In 2020, he was awarded the International Ceramics Prize for basic science by the World Academy of Ceramics. This prize is awarded quadrennially and is one of the highest in his field. The prize was awarded for "... outstanding contribution in opening new horizons in material research and specifically for your pioneering work in MAX phases and their derivatives."



Prof. Vibha Kalra is George B. Francis Chair Professor and the Director of the PhD Program in the Department of Chemical and Biological Engineering. In addition, she serves as the associate editor of Chemical Engineering Science journal since 2013. Kalra received her BS from the Indian Institute of Technology (IIT), Delhi, India, in 2004 and PhD from Cornell University in 2009, both in Chemical Engineering. Before joining Drexel in the Fall of 2010, Kalra worked in the electronic packaging research division at Intel Corporation. Her research group combines advanced material manufacturing, assembly and characterization, study of fundamental electrochemical behavior, inoperando spectroelectrochemistry, and device assembly

and testing to develop next-generation batteries and supercapacitors. She has published close to 60 peer-reviewed journal articles and has 12 pending/issued patents in the field of energy storage. Kalra is a recipient of several awards, including the NSF CAREER award (2012), ONR summer faculty fellowship (2013), AIChE DVS Outstanding Faculty of the Year Award (2015), Department of Chemical and Biological Engineering Outstanding Service Award (2018), College of Engineering Outstanding Research Award, both at assistant professor level (2015) and at midcareer level (2020), Provost Award for Outstanding Mid-Career Research Achievement (2020), and the College of Engineering Outstanding Innovation Award (2021).